Available online at www.sciencedirect.com
ScienceDirect
Geochimica et Cosmochimica Acta 71 (2007) 821–834
Geochimica
www.elsevier.com/locate/gca

X-ray absorption spectroscopy identifies calcium-uranyl-carbonate complexes at environmental concentrations ☆

Shelly D. Kelly [a,*], Kenneth M. Kemner [a], Scott C. Brooks [b]

[a] *Environmental Research Division, Argonne National Laboratory, 9700 South Cass Avenue, Argonne, IL, USA*
[b] *Oak Ridge National Laboratory, Oak Ridge, TN, USA*

Received 24 July 2006; accepted in revised form 18 October 2006

Abstract

Current research on bioremediation of uranium-contaminated groundwater focuses on supplying indigenous metal-reducing bacteria with the appropriate metabolic requirements to induce microbiological reduction of soluble uranium(VI) to poorly soluble uranium(IV). Recent studies of uranium(VI) bioreduction in the presence of environmentally relevant levels of calcium revealed limited and slowed uranium(VI) reduction and the formation of a $Ca–UO_2–CO_3$ complex. However, the stoichiometry of the complex is poorly defined and may be complicated by the presence of a $Na–UO_2–CO_3$ complex. Such a complex might exist even at high calcium concentrations, as some $UO_2–CO_3$ complexes will still be present. The number of calcium and/or sodium atoms coordinated to a uranyl carbonate complex will determine the net charge of the complex. Such a change in aqueous speciation of uranium(VI) in calcareous groundwater may affect the fate and transport properties of uranium. In this paper, we present the results from X-ray absorption fine structure (XAFS) measurements of a series of solutions containing 50 μM uranium(VI) and 30 mM sodium bicarbonate, with various calcium concentrations of 0–5 mM. Use of the data series reduces the uncertainty in the number of calcium atoms bound to the $UO_2–CO_3$ complex to approximately 0.6 and enables spectroscopic identification of the $Na–UO_2–CO_3$ complex. At nearly neutral pH values, the numbers of sodium and calcium atoms bound to the uranyl triscarbonate species are found to depend on the calcium concentration, as predicted by speciation calculations.

1. Introduction

Current remediation strategies for uranium(VI)-contaminated groundwater focus on preventing uranium migration by reducing soluble uranium(VI) to poorly soluble uranium(IV) in the form of a uranium-oxide precipitate, uraninite (Langmuir, 1978). Formation of uraninite with its very low aqueous solubility can greatly reduce the transport of uranium from contaminated areas. Dissimilatory metal reducing bacteria can rapidly reduce uranium(VI) to uranium(IV), given an appropriate electron donor (Lovley et al., 1991; Gorby and Lovley, 1992; Lovley and Phillips, 1992; Fredrickson et al., 2002; Anderson et al., 2003; Istok et al., 2004; Suzuki et al., 2004). The groundwater at many contaminated sites have complex aqueous chemistries; the effects on the rate and extent of microbial uranium(VI) reduction have not yet been fully explored (Duff et al., 2002; Brooks et al., 2003; Lovley, 2003).

Extended X-ray absorption fine structure (EXAFS) is a powerful tool for understanding the atomic coordination of uranium as a trace element incorporated into solids, adsorbed onto surfaces, and in aqueous phases. Recent EXAFS studies have characterized aqueous uranyl carbonate species (Allen et al., 1995); aqueous uranyl citrate species (Bailey et al., 2005); uranyl carbonates adsorbed onto hematite

☆ The submitted manuscript has been created by the University of Chicago as operator of Argonne National Laboratory under Contract No. W-31-109-ENG-38 with the U.S. Department of Energy. The U.S. government retains for itself, and others acting on its behalf, a paid-up, nonexclusive, irrevocable worldwide license in said article to reproduce, prepare derivative works, distribute copies to the public, and perform publicly and display publicly, by or on behalf of the government.

* Corresponding author. Fax: +1 630 252 9793.
E-mail address: skelly@anl.gov (S.D. Kelly).

0016-7037/$ - see front matter © 2006 Elsevier Inc. All rights reserved.
doi:10.1016/j.gca.2006.10.013

(Bargar et al., 2000), goethite, and natural sediments in the presence of calcium (Duff and Amrhein, 1996; Duff et al., 1997); and uranyl adsorbed onto ferrihydrite and silica gels (Reich et al., 1998). Uranyl incorporation into calcium carbonate and surface adsorption during calcite growth have also been studied by EXAFS and X-ray surface scattering (Reeder et al., 2000, 2001; Elzinga et al., 2004), and a few studies have addressed uranium naturally incorporated into calcite (Sturchio et al., 1998; Kelly et al., 2003, 2006).

Many studies have shown that calcium and carbonate have important effects on uranium geochemistry. For example, a study of the effect of calcium carbonate on uranium(VI) sorption onto soil from the Oak Ridge site (0.1% $CaCO_3$) and from the Altamont Pass, CA, site (10% $CaCO_3$) over a range of pH values showed greater adsorption to soils with lower calcium carbonate concentrations. It has been proposed that the cause of this may be formation of an aqueous $Ca_2UO_2(CO_3)_3$ complex in solution (Zheng et al., 2003). Aqueous uranyl hydroxide (pale yellow solution) sorbed onto calcium carbonate (white) powder in distilled water exhibited color changes suggesting that initial sorption of the uranyl hydroxide onto the calcite surface to form a carbonate complex (a yellow colored calcium carbonate surface) was followed by uranyl carbonate desorption forming a white calcium carbonate surface and a uncolored solution (Morse et al., 1984). Such a sequence would illustrate the affinity of uranium(VI) for aqueous calcium and carbonate. In another study related to hydroxyapatite as a permeable reactive barrier, uranyl carbonates were adsorbed to calcium on the surface of hydroxyapatite ($Ca_5(PO_4)_3OH$) (Fuller et al., 2002), demonstrating that, under some conditions, UO_2–CO_3–Ca complexes can be dominant over uranyl phosphate complexes.

In the first report of an aqueous Ca–UO_2–CO_3 complex in a study of uranium-contaminated mine tailings (Bernhard et al., 1996), the results of time-resolved laser fluorescence and ion exchange experiments led the investigators to propose that the species present was the uncharged $Ca_2UO_2(CO_3)_3^0$. The authors estimated the cumulative formation constant to be $\log\beta_{213} = 26.8 \pm 0.7$ at ionic strength 0.1 M. Kalmykov and Choppin (2000) reached a similar conclusion regarding the stoichiometry of the complex and the magnitude of the formation constant. Subsequently, Bernhard et al. (2001) made uranium edge EXAFS measurements but were unable to confirm the $Ca_2UO_2(CO_3)_3$ species, because overlapping of the calcium signal with the distant oxygen signal from the carbonate groups rendered the spectra inconclusive. In our recent study, EXAFS measurements of two solutions (50 μM uranium(VI)), 0 or 5 mM $CaCl_2$, and 30 mM HCO_3^- confirmed a Ca–UO_2–CO_3 complex in the solution with calcium; however, the EXAFS-derived uranium coordination number of calcium atoms (3.4 ± 0.9) could not be determined accurately because of the same overlap of the EXAFS signals from the calcium atoms and the distant oxygen atoms of the carbonate groups (Brooks et al., 2003).

A recent review (Guillaumont et al., 2003) questioned the weak dependence on ionic strength in some of the results presented by Kalmykov and Choppin (2000), contending that the likely existence of an as-yet-uncharacterized Na–UO_2–CO_3 complex might complicate interpretation of the Ca–UO_2–CO_3 data. Hence, no formation constant for either the Ca–UO_2–CO_3 or the Na–UO_2–CO_3 complexes has passed critical review, though the possible existence of both the Ca–UO_2–CO_3 and Na–UO_2–CO_3 aqueous species is recognized. Dong and Brooks (2006) recently reported new values of the formation constants for $CaUO_2(CO_3)_3^{2-}$ and $Ca_2UO_2(CO_3)_3^0$. These new values suggest a more prominent role for the $CaUO_2(CO_3)_3^{2-}$ species than indicated from previous studies.

Determining the number of calcium atoms bound to the uranyl carbonate system is a difficult challenge for EXAFS analysis. Nevertheless, the stoichiometry of the Ca–UO_2–CO_3 complex is important, as the net charge of the complex can change from negative $CaUO_2(CO_3)_3^{2-}$ to neutral $Ca_2UO_2(CO_3)_3^0$. This change in the aqueous speciation of uranium(VI) in groundwater could affect the fate and transport properties of uranium and on the effectiveness of bioremediation strategies (Brooks et al., 2003; Zheng et al., 2003; Davis et al., 2004; Tokunaga et al., 2004). Presented here are uranium L_{III}-edge EXAFS measurements on five solutions containing environmentally relevant concentrations of uranium(VI) and bicarbonate, with various calcium concentrations. The uranium concentration of 50 μM in these samples is similar to concentrations in contaminated groundwater at several U.S. Department of Energy sites. The samples containing environmentally relevant extended species of uranyl carbonates with calcium and sodium and could not be made at higher concentrations, because changes in ionic strength affect the uranyl species distribution. The low uranium concentrations require long integration times, even with the high brilliance of Advance Photon Source insertion device beamline MR-CAT. Although we could have obtained EXAFS spectra of higher quality for solutions with higher uranium concentrations, we considered the environmental relevance of the samples to be of greater importance. Combined modeling of the EXAFS data series enabled determination of the average uranyl species for the end member concentrations, with precision of approximately ±0.6 atom. The Na–UO_2–CO_3 species was spectroscopically confirmed, and the numbers of calcium and sodium atoms bound to the uranyl triscarbonate species were shown to depend on the calcium concentration and to be more consistent with equilibrium aqueous speciation models based on the formation constants from recent anion exchange studies (Dong and Brooks, 2006).

2. Materials and methods

2.1. Sample chemistry and speciation calculations

The base solution for EXAFS measurements consisted of 30 mM $NaHCO_3$ under a headspace of N_2/O_2 (80:20),

pH 6.9, with 50 μM uranium(VI) as uranyl acetate. Separate samples were prepared for each EXAFS measurement. In addition to a no-calcium control sample, EXAFS measurements were made for three calcium concentrations via the addition of $CaCl_2$: 50 μM (Ca50), 500 μM (Ca500), and 5000 μM (Ca5000). Acetate (5 mM, $NaC_2H_3O_2$), a common electron donor for uranium(VI) reduction studies, was added to the no-calcium sample (Ca0a) and one of the Ca5000 samples (Ca5000a). Equilibrium geochemical speciation calculations indicated that all solutions were under-saturated with respect to U(VI) solids under our experimental conditions. In agreement with these predictions, no uranyl solid phase was detected in the measured EXAFS. Preliminary tests on similar systems showed that uranyl adsorption to the containers is minimal under our experimental conditions.

The predicted uranium(VI) aqueous species distribution in the solutions was calculated by using the React module in the commercially available software program The Geochemist's Workbench (Bethke, 2005). Formation constants for the inorganic uranium(VI) complexes were obtained from the extensive compilation of the Nuclear Energy Agency (NEA; Grenthe et al., 1992; Guillaumont et al., 2003), while those for the uranyl acetate complexes were from Shock and Koretsky (Shock and Koretsky, 1993). Formation constants for the Ca–UO_2–CO_3 complexes $CaUO_2(CO_3)_3^{2-}$ and $CaUO_2(CO_3)_3^{0}$ are not officially accepted by the NEA database reviewers. Although the existence of the complexes is not questioned, work to resolve concerns related to experimental procedure and data analysis continues (e.g., Dong and Brooks, 2006). In keeping with the recommendation of the NEA reviewers, the formation constants proposed by Bernhard et al. (2001) were used for the speciation calculations:

$$\begin{aligned} &Ca^{2+} + UO_2^{2+} + 3CO_3^{2-} \leftrightarrow CaUO_2(CO_3)^{2-} \\ &\quad \log\beta_{113} = 25.4 \\ &2Ca^{2+} + UO_2^{2+} + 3CO_3^{2-} \leftrightarrow Ca_2UO_2(CO_3)^{0} \\ &\quad \log\beta_{213} = 30.55 \end{aligned} \tag{1}$$

In addition, the speciation calculations were also performed using the values recently determined by Dong and Brooks (2006): $\log\beta_{113} = 27.18$ and $\log\beta_{213} = 30.70$. The predicted average number of calcium atoms associated with uranium was calculated as

$$\frac{2[Ca_2UO_2(CO_3)_3^{0}] + [CaUO_2(CO_3)_3^{2-}]}{[U]_{total}}, \tag{2}$$

where [] denotes molar concentration. This calculation is consistent with the nature of the EXAFS signal that is collected, which represents the weighted average local environment of all uranium species in the sample. Under all experimental conditions, four aqueous species, $UO_2(CO_3)_3^{2-}$, $UO_2(CO_3)_3^{4-}$, $CaUO_2(CO_3)_3^{2-}$, and $Ca_2UO_2(CO_3)_3^{0}$, are predicted to constitute greater than 99.5% of the total U(VI).

2.2. Uranium L_{III}-edge EXAFS measurements

The uranium concentration in our samples (50 μM) is similar to the level of uranium contamination at the U.S. Department of Energy's Natural and Accelerated Bioremediation Field Research Center site, Oak Ridge National Laboratory, TN, USA (2000). The transmission X-ray absorption edge step height is proportional to the number of uranium atoms in the sample volume (approximately 3 mm^3) exposed to the X-ray beam. In concentrated samples, the element of interest typically constitutes a large percent (10–100%) of the total number of atoms in the sample. Such samples are measured in transmission mode and are prepared to have an ideal transmission edge step height of approximately 1.0 (Stern and Heald, 1983). Samples that have the element of interest present at about 1–10% of the total number of atoms within the sample typically are measured in fluorescence mode and often have a transmission edge step height of approximately 0.01–0.1. The uranium concentrations in the samples of this study were extremely dilute in comparison to those in a typical fluorescence measurement, with only 1 uranium atom for every 10^7 atoms (10^{-5}%). Consequently, the transmission edge step heights for these samples were approximately 2×10^{-4}.

Because of the extremely low uranium concentrations of our samples, we used several special experimental procedures. These uranium L_{III}-edge measurements were made at the high-photon-flux ($\sim 5 \times 10^{13}$ photons per second) insertion device (10-ID) beamline, MR-CAT (Segre et al., 2000), at the Advance Photon Source, with the use of a 13-element solid-state detector (Canberra with XIA electronics). The insertion device was tapered to reduce the variation in the X-ray intensity to less than 15% throughout the scanned energy range (17,000–18,000 eV). A silicon(111) double-crystal monochromator was used to select the X-ray energy. A rhodium mirror was used to eliminate X-rays with higher harmonic energies. The incident X-ray intensity was monitored through use of a nitrogen-filled ion chamber. The XAFS signal was integrated for long periods of time (1 h per scan or ~15 s per data point), and several data sets were collected from each of the samples and averaged to increase the signal-to-noise ratio (Table 1).

The data were processed with the UWXAFS (Stern et al., 1995) software package by using standard procedures. The background was removed with Rbkg = 1.0 Å (Newville et al., 1993), from each data set, and the resulting fine structure spectra [$\chi(k)$ data] were averaged (Fig. 1). Theoretical models were constructed with the program FEFF7 (Zabinsky et al., 1995) and the crystallographic atomic positions of liebigite (Mereiter, 1982) with calcium atoms coordinated to the uranyl-triscarbonate moiety and andersonite (Coda et al., 1981) with both sodium and calcium coordinated to the uranyl-triscarbonate

Table 1
Description of the EXAFS data collected

Sample	Number of scans	Data range ($Å^{-1}$)	Number of independent points	
			$\Delta R = 1$–4 Å	$\Delta R = 2.9$–4 Å
Ca5000a	3	3.5–7.5	9.5	4.7
Ca5000	10	3.5–9.5	13.3	6.0
Ca500	8	3.5–9.5	13.3	6.0
Ca50	6	3.5–8.5	11.4	5.3
Ca0a	10	3.5–8.0	10.4	5.0
Liebigite		3.0–12.0	20.8	

Each scan represents 1 h of data collection time. The data ranges listed are the portion of the data used in the Fourier transform.

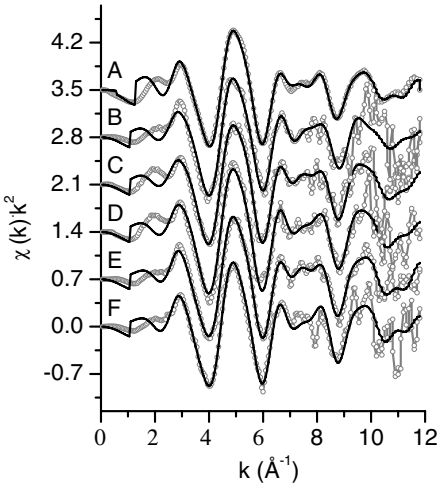

Fig. 1. Averaged $\chi(k) \cdot k^2$ data (open symbols) and modeled data (solid line) for liebigite (A), Ca0a (B), Ca50 (C), Ca500 (D), Ca5000 (E), and Ca5000a (F) samples.

moiety. Automatic overlapping of the muffin tin potentials was used in the FEFF7 calculation. The liebigite standard EXAFS spectrum is from Catalano and Brown (2004).

2.3. EXAFS data analysis

X-ray absorption data [$\mu(E)$] were collected as a function of incident X-ray energy through the U L_{III} absorption edge of 17,166 eV, from approximately 17,000 to 18,000 eV. The step-like absorption function at the uranium L_{III}-edge was removed from the data by using Athena (Ravel and Newville, 2005) and IFEFFIT (Newville, 2001) programs. The threshold energy (E_0) was chosen to define the excited photoelectron wave number (k), given by $k^2 = E_0(2m_e/h^2)$, where m_e is the mass of an electron, and h is Planck's constant. The value for the threshold energy was modified during the fitting procedure by allowing determination of ΔE, an energy shift parameter. The resulting EXAFS $\chi(k)$ spectrum was weighted by k raised to the power of 1, 2, or 3 (referred to as the k weight). The EXAFS $\chi(k)$ spectrum is a sum of sinusoidal functions (Stern, 1974) due to groups of neighboring atoms (a shell of atoms) at approximately the same distance from the uranium atoms in the sample. For a single scattering event of the photoelectron, the frequency is closely related to the bond length between the uranium atom and its neighbors. The amplitude of each component is related to the numbers and types of neighboring atoms.

The EXAFS $\chi(k)$ spectrum is Fourier transformed from wavenumber ($Å^{-1}$) to radial distance (Å) to separate the sinusoidal components. The Fourier transform (FT) yields a complex function of R. Maxima in the magnitude of the FT represent the signals from each shell of atoms about the uranium atoms. The heights and positions of these maxima are related to: (1) the types and numbers of neighboring atoms and (2) the distances between the uranium atoms and their neighboring atoms, respectively. Therefore, each shell of atoms (all atoms of the same type and at the same distance) contributes to the shape and height of one peak in the magnitude of the FT of the EXAFS spectrum.

EXAFS scattering paths originate at the absorbing atom, go to one or more neighboring atoms, and return to the absorbing atom. The theoretical models of the experimental EXAFS data are made by summing the contributions from scattering paths of the photoelectron from the different shells of atoms. Most of the EXAFS parameters are related to the physical description of the scattering paths from which the models are built. These parameters include the types of neighboring atoms that define the scattering path, the number of identical paths (N), the half path length (R), and the mean-squared deviation (σ^2) of the half path length R. For a single scattering path, these parameters are the average number (N) and type of atoms around the uranium atoms in the sample, with a given radial distance (R) and a mean-squared deviation (σ^2) of that distance.

3. Results

3.1. Speciation calculations

In the absence of calcium, $UO_2(CO_3)_3^{4-}$ and $UO_2(CO_3)_3^{2-}$ are predicted to be the dominant aqueous species; however, they decrease in importance as the concentration of calcium in solution increases and $Ca_2UO_2(CO_3)_3^0$ increases concomitantly (Table 2). If the Ca–U–CO_3 species are minor components of the solution and independent of the calcium concentration, then the EXAFS results should reflect a small and invariant number of calcium atoms in close association with uranium. Conversely, if the predicted aqueous speciation trend is correct, then the EXAFS analysis is expected to reflect an increase in the number of calcium atoms associated with uranium as the calcium concentration increases. The predicted average number of sodium atoms associated with uranium was calculated similarly to that for calcium (Eq. (2)), but with the assumption of four sodium atoms per $UO_2(CO_3)_3^{4-}$, two sodium atoms per $UO_2(CO_3)_3^{2-}$, and two sodium atoms

Table 2
Predicted uranium(VI) aqueous species distribution for the conditions of the EXAFS measurements at pH 6.9

	Mol% total uranium(VI)								
	Ca0a	Ca50		Ca500		Ca5000		Ca5000a	
Model version[a]		A	B	A	B	A	B	A	B
Aqueous species									
$UO_2(CO_3)_3^{4-}$	92.46	89.40	63.42	37.82	10.94	0.91	0.5	1.12	0.60
$UO_2(CO_3)_3^{2-}$	7.45	7.93	5.64	3.30	0.96	0.07	0.03	0.07	0.04
$Ca_2UO_2(CO_3)_3^{0}$		1.59	0.81	55.10	22.72	98.32	76.22	98.06	74.86
$CaUO_2(CO_3)_3^{2-}$		0.98	30.06	3.73	65.38	0.70	23.24	0.75	24.50
Avg # Na per U (N_{Na})[b]	3.85	3.77	3.25	1.65	1.76	0.04	0.49	0.06	0.51
Avg # Ca per U (N_{Ca})[b]	0	0.04	0.32	1.14	1.11	1.97	1.76	1.97	1.74

[a] Model version A uses the Ca–UO_2–CO_3 stability constants reported by Bernhard et al. (2001) and version B uses the stability constants reported by Dong and Brooks (2006).
[b] See text (Section 3.1) for a description of this calculation.

per $CaUO_2(CO_3)_3^{2-}$ (Table 2). For most of the samples, the speciation calculations for Model A (with the Ca–UO_2–CO_3 stability constants reported by Bernhard et al. (2001)) and for Model B (with the Ca–UO_2–CO_3 stability constants reported by Dong and Brooks (2006)) have average values for the number of sodium or calcium atoms per uranium atom differing by less than half an atom (Table 2).

3.2. Building the EXAFS model

Speciation calculations predicted that the dominant species in the solutions without calcium and the remaining species in the samples with calcium are uranyl triscarbonate [$UO_2(CO_3)_3^{4-}$], with or without calcium (Table 2). This species has four shells of atoms surrounding the uranium atom. The two axial oxygen (O_{ax}) atoms of the uranyl form the first shell of atoms. The atoms from the three carbonate groups, including six equatorial oxygen (O_{eq}) atoms, three carbon atoms, and three distant oxygen (O_{dist}) atoms (Fig. 2), form the next three shells of atoms. The coordination numbers for these shells were not determined in the fit to the EXAFS data, but rather they were held at values of 6, 3, and 3 for the O_{eq}, carbon, and O_{dist} shells, on the basis of the speciation calculations. Important linear multiple scattering (MS) paths from the O_{ax1}–U–O_{ax2} and U–C–O_{dist} atoms are included in the EXAFS model.

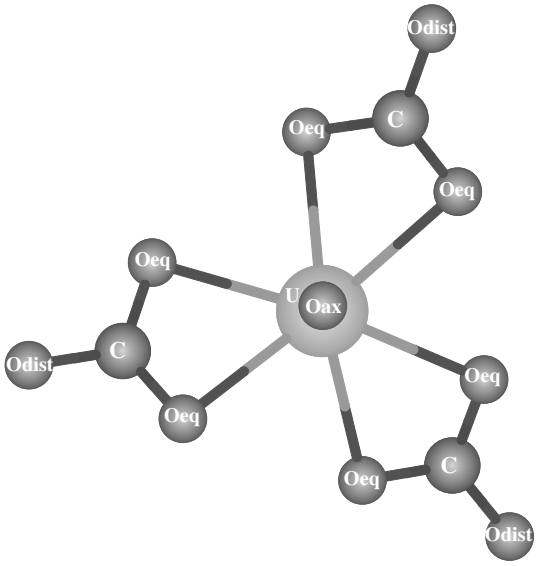

Fig. 2. Ball-and-stick figure of $(UO_2)(CO_3)_3$ species. The uranyl moiety (UO_2) is made up of a uranium atom bound to two axial oxygen (O_{ax}) atoms above and below the uranium atom.

Table 3 lists the scattering paths included in the model and defines their parameterization. The paths shown describe the atoms that contribute to the EXAFS signal. For example, U–O_{ax} represents a path that starts at a uranium atom, goes to an O_{ax} atom, and returns to the original uranium atom. The number of paths is the number of identical paths for the $UO_2(CO_3)_3^{4-}$ complex. The path distances shown in Table 3 are the original path lengths (bond lengths for single scattering paths) based on the structure of liebigite. The subscripts on the EXAFS parameters Δr (change in the half path length), σ^2 (mean-squared deviation of the half path length), and ΔE (energy shift of the photoelectron) indicate their parameterization.

The MS paths do not increase the number of fitting parameters, as the parameters for the MS paths are determined from the corresponding single scattering paths (see Table 3). Some previous EXAFS studies of the UO_2^{2+} moiety either have not discussed the O_{ax1}–U–O_{ax2} MS paths (Waite et al., 1994; Bernhard et al., 2001) or have concluded that these paths could be neglected (Bostick et al., 2002; Dodge and Francis, 2003). Inspection of these paths in $\chi(k)$ indicates that the majority of their contribution is at k values less than 4 $Å^{-1}$. If this region of the data is not used in the analysis, these paths should not be necessary. However, the FT data range used in our analysis starts at $k = 3.0 - 3.5$ $Å^{-1}$, and thus these MS paths were included.

To account for sodium and calcium atoms that could be bound to the uranyl carbonate system, the model includes U–Ca and U–Na paths. On the basis of other Ca/Na–UO_2–CO_3 systems, the approximate distances expected are 3.8–4.1 Å for U–Ca (Coda et al., 1981; Mereiter, 1982; Reeder et al., 2000; Bernhard et al., 2001; Rakovan et al., 2002; Kelly et al., 2003, 2006) and 3.7–3.9 Å for U–Na (Coda et al., 1981; Ondrus et al., 2003). These paths were

Table 3
Description of the EXAFS model applied to the liebigite data and the Na/Ca–UO_2–CO_3 solution data

Path	Number of paths	Distance (Å)	Δr	σ^{2a}	ΔE
U–O_{ax}	2	1.8	$\boldsymbol{\Delta r_{oax}}$	$\boldsymbol{\sigma^2_{oax}}$	$\boldsymbol{\Delta E_1}$
U–O_{eq}	6	2.4	$\boldsymbol{\Delta r_{oeq}}$	$\boldsymbol{\sigma^2_{oeq}}$	$\boldsymbol{\Delta E_2}$
U–C	3	2.9	$\boldsymbol{\Delta r_c}$	$\boldsymbol{\sigma^{2\,a}_c}$	ΔE_2
U–O_{ax1}–O_{ax2}	2	3.6	$2 \cdot \Delta r_{oax}$	$2 \cdot \sigma^2_{oax}$	ΔE_1
U–O_{x1}–U–O_{ax2}	2	3.6	$2 \cdot \Delta r_{oax}$	$2 \cdot \sigma^2_{oax}$	ΔE_1
U–O_{ax1}–U–O_{ax1}	2	3.6	$2 \cdot \Delta r_{oax}$	$4 \cdot \sigma^2_{oax}$	ΔE_1
U–O_{dist}	3	4.2	$\boldsymbol{\Delta r_{odist}}$	$\boldsymbol{\sigma^2_{odist}}$ [a]	ΔE_2
U–C–O_{dist}	6	4.2	Δr_{odist}	σ^2_{odist} [a]	ΔE_2
U–C–O_{dist}–C	3	4.2	Δr_{odist}	σ^2_{odist} [a]	ΔE_2
U–Ca	$\boldsymbol{N_{Ca}}$ [b]	4.1	$\boldsymbol{\Delta r_{ca}}$	$\boldsymbol{\sigma^2_{ca}}$ [a]	ΔE_2
U–Na[c]	$\boldsymbol{N_{Na}}$	3.7–3.9	$\boldsymbol{\Delta r_{na}}$	σ^2_{ca} [a]	ΔE_2

Parameters in bold type were optimized to fit the model to the data.
[a] σ^2 values were determined from the liebigite EXAFS results for the model of the Na/Ca–UO_2–CO_3 solutions.
[b] The coordination for N_{Ca} was held at 3 for the model of liebigite EXAFS data.
[c] The U–Na path was not included in the model of the liebigite EXAFS data or in the model +Ca−Na.

added to the model (Table 3). The Na/Ca–UO_2–CO_3 model requires the determination of 15 variables to describe the EXAFS signal from a uranyl triscarbonate complexed with an unknown number of sodium and/or calcium atoms.

3.3. EXAFS model applied to liebigite

The Ca–UO_2–CO_3 model (without sodium) was applied to EXAFS data for the well-known crystal structure of liebigite, $Ca_2UO_2(CO_3)_3$ (Mereiter, 1982). The liebigite EXAFS spectrum contains 21 independent data points, as calculated from the Fourier-transformed data range (3.0–12.0 $Å^{-1}$) and the modeled region (1–4 Å) of the data (Table 1). The paths included in the model and the 13 parameters optimized (bold type) are listed in Table 3. Fig. 3 shows the magnitude and real part of the Fourier transform (FT) of the liebigite data and the model processed with a k weight of 2, with the contribution from each scattering path in the model (where the importance of the MS paths is illustrated qualitatively). The best-fit values for the variables determined from the fit to these data are listed in Table 4. Also determined in the fit were $\Delta E_1 = 2.6 \pm 2.1$ eV and $\Delta E_2 = 7.0 \pm 2.3$ eV as defined in Table 3. The value for S_0^2 was held at 1.0; the true value was found to be consistent with this assumed value with an uncertainty of 10%. This value for S_0^2 was used in the EXAFS model of the Na/Ca–UO_2–CO_3 solution series, and the uncertainty in S_0^2 was added in quadrature to the uncertainties in coordination number determined from the solution series EXAFS data.

3.4. EXAFS model applied to the Na/Ca–UO_2–CO_3 data series

3.4.1. Liebigite model applied to Na/Ca–UO_2–CO_3 data series (Model +Ca−Na)

The data series for the solution samples (Ca0a, Ca50, Ca500, Ca5000, Ca5000a) was initially refined with the liebigite model (model +Ca−Na). The EXAFS parameters for σ^2 of the U–C, U–O_{dist}, and U–Ca paths were used from the liebigite refinement (which excluded the

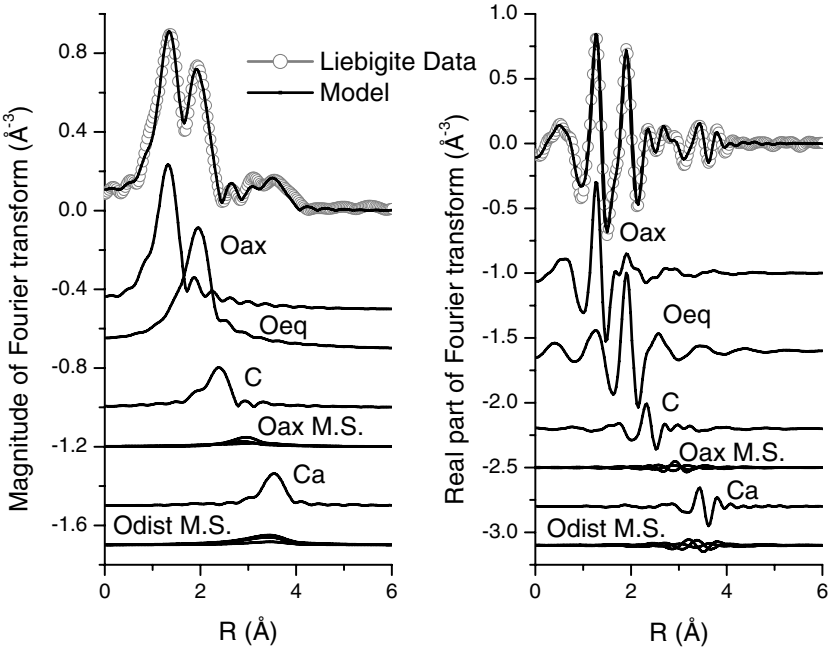

Fig. 3. The magnitude and real part of the Fourier transform of the liebigite spectrum and model processed with a k weight of 2. The data and model are shown at the top of each panel as open symbols and a solid line, respectively. Beneath the data and model are the individual contributions to the total model from each path in the model.

Table 4
EXAFS results and parameters from the liebigite data and the Na/Ca–UO_2–CO_3 aqueous data

Path	Number of paths	Liebigite results		Na/Ca–UO_2–CO_3 results Model +Ca+Na	
		R (Å)	σ^2 ($\times 10^{-3}$ Å^2)	R (Å)	σ^2 ($\times 10^{-3}$ Å^2)[a]
U–O_{ax}	2	1.792 ± 0.009	3.3 ± 0.5	1.78 ± 0.01	σ^2_{oax}
U–O_{eq}	6	2.45 ± 0.02	8.4 ± 0.8	2.45 ± 0.01	σ^2_{oeq}
U–C	3	2.89 ± 0.01	3 ± 2	2.89 ± 0.01	3
U–O_{ax1}–O_{ax2}	2	3.59 ± 0.02	13 ± 2	3.57 ± 0.02	$4 \cdot \sigma^2_{oax}$
U–O_{x1}–U–O_{ax2}	2	3.62 ± 0.02	7 ± 1	3.57 ± 0.02	$2 \cdot \sigma^2_{oax}$
U–O_{ax1}–U–O_{ax1}	2	3.62 ± 0.02	7 ± 1	3.57 ± 0.02	$2 \cdot \sigma^2_{oax}$
U–Na	N_{nai}[a]	N/A	N/A	3.84 ± 0.03[c]	4
U–Ca	N_{cai}[a,b]	4.04 ± 0.02	4 ± 2	4.02 ± 0.02	4
U–O_{dist}	3	4.13 ± 0.10	24 ± 17	4.11 ± 0.07	24
U–C–O_{dist}	6	4.14 ± 0.10	24 ± 17	4.11 ± 0.07	24
U–C–O_{dist}–C	3	4.14 ± 0.10	24 ± 17	4.11 ± 0.07	24

Values without uncertainties were held constant at the given value.
[a] The EXAFS parameters for σ^2 of the U–O_{ax} and U–O_{eq} paths and the number of U–Na and U–Ca paths were determined independently (see Table 6) for each data set in the Na/Ca–UO_2–CO_3 model.
[b] The number of U–Ca paths was held at 3 for the liebigite model.
[c] The distance of the U–Na signal for the spectra without calcium, Ca0a, was determined independently from the spectra with calcium and found to be 3.82 ± 0.003 Å.

possibility of a Na–UO_2–CO_3 complex). Use of a crystal structure for σ^2 values of an aqueous complex is not ideal but is justified here on the basis of uncertainties in the measured spectra. Clearly, EXAFS data of higher quality, which could be obtained from solutions with higher uranium concentrations, could help determine the σ^2 values independently of the liebigite structure. The disadvantage is that the uranium concentration would no longer be environmentally relevant. We believe that the environmental relevance of the samples is more critical than independent determination of these σ^2 values. The solution samples and hence the measured spectra are very similar (Fig. 1) and are expected to have many parameters in common. To determine these common parameters, each data set was modeled independently. Parameters found to overlap within the uncertainties (Δr and ΔE_0 values) were constrained to a single value for all five data sets. This did not imply that these values were the same for all data sets, but rather that the values were so similar that our measurement was insensitive to the differences. The model described in Table 3 contains 8 common parameters (6 Δr values and 2 ΔE_0 values) refined simultaneously to all 5 spectra, plus 3 independent parameters (σ^2_{oax}, σ^2_{oeq}, and N_{Ca}) refined to each spectra independently of the other spectra, giving an average number of approximately 5 (8 common parameters/5 data sets + 3 independent parameters) variables per spectra. This model is reasonable for our data, because the Fourier-transformed data range (see Table 1) and the modeled data region from 1 to 4 Å give approximately 10–14 independent points in each data set.

The best-fit values for the number of calcium atoms bound to the uranyl triscarbonate complex (N_{Ca}; Table 5), determined by using the model +Ca−Na, do not show the expected dependence on calcium concentration. Equilibrium aqueous speciation calculations indicate that the value of N_{Ca} is expected to increase from 0 to 2 as the calcium concentration increases from 0–50 to 500–5000 μM. The best-fit values are consistent with two calcium atoms over the entire data series, whereas the speciation modeling (Table 2) indicated that N_{Ca} should increase with calcium concentration. However, formation of the hypothesized Na–UO_2–CO_3 complex was not properly accounted for in this model. Therefore, the model was modified to allow for a Na–UO_2–CO_3 complex.

Table 5
Results for the number of sodium and calcium atoms from the simultaneous fit to all 5 data sets determined by consecutively more refined models

Path	Ca0a	Ca50	Ca500	Ca5000	Ca5000a
Model +Ca−Na, fit region from 1 to 4 Å					
U–Ca	—	2.1 ± 0.6	2.0 ± 1.0	2.2 ± 0.5	1.8 ± 0.5
Model +Ca+Na, fit region from 1 to 4 Å					
U–Na	3.2 ± 1.2	3.1 ± 3.1	2.3 ± 4.4	0.0 ± 2.3	
U–Ca	—	0.4 ± 1.9	0.9 ± 2.7	2.4 ± 1.3	2.3 ± 1.4
Model +Ca+NaOnly, fit region from 2.9 to 4 Å					
U–Na	3.2 ± 0.7	2.8 ± 1.7	2.3 ± 2.3	0.8 ± 1.0	
U–Ca	—	0.6 ± 1.1	0.9 ± 1.5	2.0 ± 0.6	1.9 ± 0.6

3.4.2. Liebigite with sodium model applied to the Na/Ca–UO_2–CO_3 data series (Model +Ca+Na)

The addition of a U–Na path to the liebigite model (model +Ca+Na) introduced three new parameters (Δr, σ^2, and N_{Na}) to the model of the solution series EXAFS spectra. The EXAFS σ^2 value for the U–Na path was held at the value for the U–Ca path based on the liebigite standard at approximately the same radial distance. This constraint was initially tested by allowing the O_{dist}, sodium, and calcium σ^2 values to be determined.

Table 6
σ^2 values for the U–O_{ax} and U–O_{eq} paths from simultaneous fitting using the model +Ca+Na, which includes both the sodium and calcium signals, to all five data sets, over the full fitting region of 1–4 Å

EXAFS variable	Ca0a	Ca50	Ca500	Ca5000	Ca5000a
σ^2_{Oax} ($\times 10^{-3}$ Å^2)	3.4 ± 1.0	1.8 ± 0.7	2.3 ± 1.1	1.4 ± 0.5	2.7 ± 0.7
σ^2_{Oeq} ($\times 10^{-3}$ Å^2)	7.3 ± 1.1	7.8 ± 1.0	6.0 ± 1.2	7.9 ± 0.8	5.9 ± 0.8

Specifically, the σ^2 values determined for the O_{dist}, calcium, and sodium shells by modeling the data series are 0.019 ± 0.020, 0.005 ± 0.009, and 0.001 ± 0.012 Å^2, respectively. These results lend some confidence in our constraint of the σ^2 values for the O_{dist} and calcium shells to the values determined from the liebigite standard, because the O_{dist} σ^2 value of 0.019 ± 0.020 Å^2 and the calcium σ^2 value of 0.005 ± 0.009 Å^2 are consistent with the values determined for the liebigite standard (0.024 ± 0.017 Å^2 for the O_{dist} shell and 0.004 ± 0.002 Å^2 for the calcium shell). The best-fit σ^2 value from the solution series for the sodium shell (0.001 ± 0.010 Å^2) is not within the acceptable range for σ^2 values (0.003–0.030 Å^2). Furthermore, the sodium bond strength (as measured by the sodium shell σ^2 value of ~0.001 Å) is unlikely to be larger than the calcium bond strength (as measured by the calcium shell σ^2 value of ~0.005 Å), because the bond strength generally increases with increasing anion–cation charge transfer.

The effect on the bond strength with more single charged sodium atoms (4 Na^+ atoms), as compared to fewer doubly charged calcium atoms (2 Ca^{2+} atoms) bound to the $UO_2(CO_3)_3^{4-}$ moiety, would suggest that the $UO_2(CO_3)_3^{4-}$–Na_4^{4+} bond is weaker than the $UO_2(CO_3)_3^{4-}$–Ca_2^{4+} bond. This effect is not too large, because modeling of the solution series EXAFS data did not result in a larger σ^2 value for the sodium shell than for the calcium shell. Because the sodium shell σ^2 value was found to be unrealistically small but consistent (within the uncertainties) with the σ^2 value for the calcium shell, the sodium shell and calcium shell σ^2 values were constrained to the value of 0.004 Å^2 determined for the liebigite standard.

The EXAFS model was modified by adding a Δr value for the sodium signal to the common parameters for the spectra with calcium. An independent Δr value for the sodium signal of the spectrum without calcium significantly improved the quality of the fit to the data series. The number of sodium atoms bound to the uranyl triscarbonate (N_{Na}) was determined independently for each spectrum except for Ca5000 and Ca5000a. The same N_{na} was optimized for both of these two (Ca5000 and Ca5000a) spectra. The model +Ca+Na results in approximately 6 (9 common parameters/5 data sets + 4 independent parameters) variables per data set which is less than the number of independent points, as each data set contains approximately 10–14 independent points (Table 1). The spectrum without Ca includes one more independent variable Δr_{Na}. The best-fit values for N_{Ca} and N_{Na}, determined by using the model

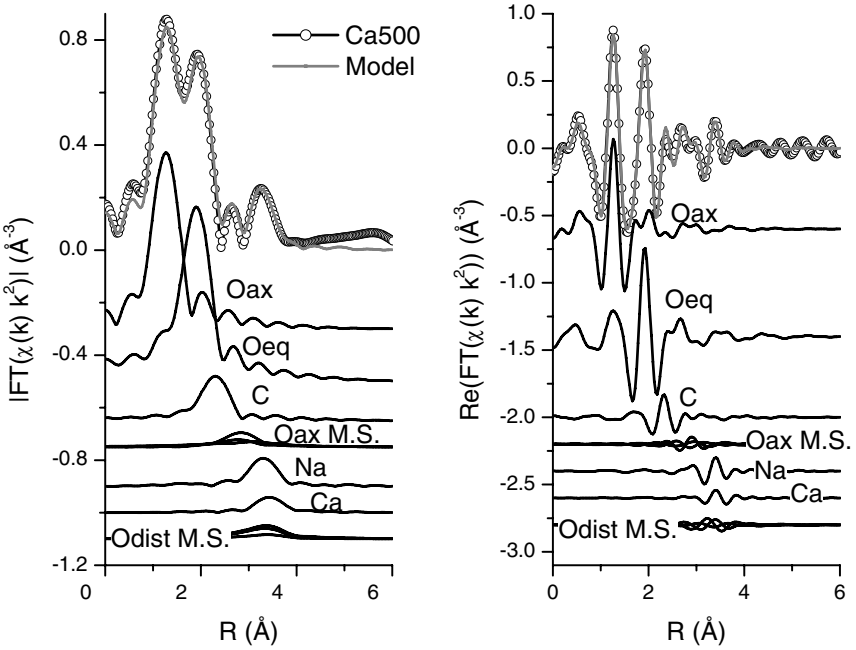

Fig. 4. The magnitude and real part of the Fourier transform of the Ca500 data and model +Ca+Na processed with a k weight of 2. The data and model fit are shown at the top of each panel as open symbols and a solid line, respectively. Beneath the data and fit are the individual contributions to the total model from each path in the model.

+Ca+Na, show dependence on the calcium concentration (Table 5). As expected, N_{Na} decreases with increasing calcium concentration, while N_{Ca} increases with increasing calcium concentration.

The best-fit values for the other EXAFS parameters (R and σ^2) are listed in Table 4. In addition to these parameters, two energy shift parameters ΔE_1 and ΔE_2 (see Table 3) were optimized to the values of -0.8 ± 1.6 and 4.4 ± 1.9 eV, respectively. Fig. 4 illustrates the FT of the Ca500 data, the total model, and the contribution to the model from each path. This data set was chosen because of the strong sodium and calcium signals at the 500 μM calcium concentration. Fig. 4 illustrates the isolation in the FT of the calcium and sodium signals (2.9–4 Å) from the O_{ax}, O_{eq}, and carbon signals (1.0–2.9 Å).

Inclusion of possible neighboring sodium atom(s) in the model results in an increasing N_{Ca} and decreasing N_{Na}, as expected with increasing [Ca]; however, the uncertainties in the coordination numbers are large. The uncertainty in N_{Ca} will be larger when optimizing the model to the EXAFS data over the entire fit region (1–4 Å) than for a smaller subregion (2.9–4 Å) where the sodium/calcium signal dominates. To minimize the uncertainty in the EXAFS variables, the method used to calculate uncertainties needs to be understood qualitatively. The EXAFS uncertainties were calculated on the basis of procedures in *Standardized Data Reduction and Error Analysis for the Physical Sciences* (Bevington and Robinson, 1992). The implementation of these procedures for EXAFS analysis is described elsewhere (Stern et al., 1995; Newville et al., 1999).

Briefly, the uncertainty in each parameter is determined by iteratively changing the parameter's value and re-optimizing all of the other parameters until the chi-squared value of the fit increases by 1 (Stern et al., 1995). The amount of change in the parameter required to increase the chi-squared value is the reported uncertainty in the parameter. The chi-squared value is proportional to the sum of the square of the differences between the model and the data over the entire fit region divided by the number of data points within the fit region. If the fit region includes a portion of the model that is not affected by the calcium signal, and if this portion of the fit has a larger or smaller average misfit, then the uncertainty in N_{Ca} obtained by increasing the chi-squared value will not be accurate. Reducing the fit region to 2.9–4.0 Å makes the chi-squared value for the fit a more accurate measure of the misfit of the model in the region affected by the calcium signal. As a result, the uncertainty will be a measure of the ability of the model to accurately reproduce the data in the affected region. Furthermore, reducing the fit region will reduce the uncertainty in the N_{Ca} atoms, because smaller changes in N_{Ca} will result in larger changes in the chi-squared value for the fit of the reduced data range. The chi-squared value for the subregion (2.9–4 Å) is affected by changes in N_{Ca} at every data point, whereas the chi-squared value for the entire fit region (1–4 Å) is affected by changes in N_{Ca} at less than half ($[4 - 2.9]/[4 - 1]$) of the data points. Hence, to minimize the uncertainty in the EXAFS parameters, the fit region needs to match the region affected by the parameters determined in the fit.

3.4.3. Liebigite with the sodium model applied to the Na/Ca–UO_2–CO_3 data series optimized in the region where only the calcium and sodium signals contribute (Model +Ca+NaOnly)

The initial EXAFS model was used to describe the data range from 1 to 4 Å, but the EXAFS signal from sodium and calcium atoms dominates in the subregion from 2.9 to 4 Å. Because the U–Na and U–Ca radial distances are significantly different from the U–O_{ax}, U–O_{eq}, and U–C distances, the region of the FT corresponding to the U–Na and U–Ca distances (2.9–4.0 Å) can be modeled separately. To do this, the parameters from the O_{ax}, O_{eq} and carbon signals were held to the values determined previously, and the model was optimized in the subregion from 2.9 to 4 Å, where the sodium and calcium signals dominate.

Reducing the fit region is similar to Fourier filtering of the EXAFS data to model only the signals that contribute within a particular region in the FT spectrum; however, our method explicitly accounts for the overlap of the U–O_{eq} tail and the U–O_{ax} MS paths within our modeled subregion (see Fig. 4), whereas Fourier filtering of the EXAFS data would not. The U–O_{eq} tail and the U–O_{ax} MS paths have significant contributions in the subregion from 2.9 to 4 Å, as compared to the U–Ca, U–Na, and U–O_{dist} signals, but the U–O_{eq} tail and the U–O_{ax} MS signals are defined by the data outside the subregion from 2.9 to 4 Å, where the U–O_{ax} and U–O_{eq} signals dominate between 1 and 2.9 Å.

The correlations between the parameters that describe the model outside the subregion (U–O_{eq} and U–O_{ax}) — as compared to the parameters that describe the model within the subregion (U–Ca, U–Na, and U–O_{dist})—were calculated from the previous optimization of the model to the entire data range from 1 to 4 Å. All correlations between the parameters from the outside region (U–O_{eq} and U–O_{ax}) and the parameters from the inside region (U–Ca, U–Na, and U–O_{dist}) were determined to be less than 34%. To put this small correlation into perspective, the correlation between N_{Ca} (an amplitude term) and the energy shift parameter for the Ca shell (a phase term) is generally agreed to be small, and its correlation of 36% is similar to the correlation between the parameters that describe the outside region (U–O_{eq} and U–O_{ax}), rather than those that describe the inside region (U–Ca, U–Na, and U–O_{dist}). In contrast, the correlation between N_{Na} and N_{Ca} is large (~92%). The model explicitly accounts for this large correlation as the large uncertainty in the reported values for N_{Na} and N_{Ca}.

The model +Ca+NaOnly include 3 common parameters (Δr for the U–Na, U–Ca, and U–O_{dist} signals) for all 5 data sets and 2 independent parameters (N_{Na} and N_{Ca}), giving approximately 3 variables ($3/5 + 2$) per data set. The spectrum without Ca includes one more independent parameter

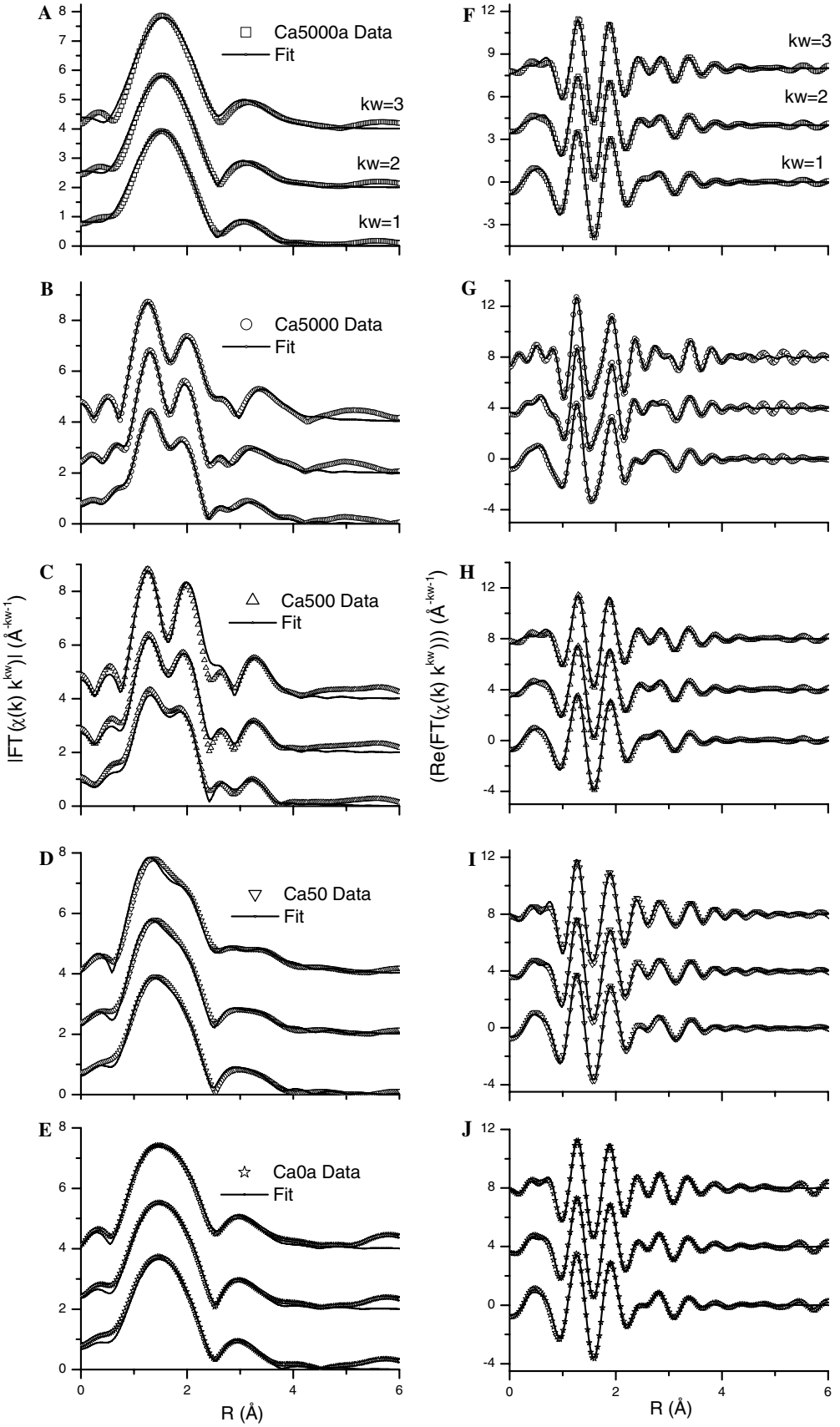

Fig. 5. The magnitude (A–E) and real part (F–J) of the Fourier transform, processed with k weights of 1, 2, and 3, for all five spectra, with Model Fits. Model +Ca+NaOnly was simultaneously optimized to each of these data sets, processed with k weights of 1, 2, and 3. The data processed with k weights of 1 and 2 are rescaled, so that the first peak height is similar to that of data processed with k weight of 3.

Δr for the U–Na signal. Each data set contains approximately 5–6 independent points (Table 1). The effect of increasing the ratio of the number of independent points to the number of variables is to reduce the uncertainties in the determined variables (assuming that the model has enough freedom to reproduce the data).

The model +Ca+NaOnly is refined to the data by processing the data with k weights of 1, 2, and 3. The plots of the FT of all of the data and the best-fit models for all three k weights (shown in Fig. 5) indicate that the model accurately reproduces the measured spectra. The agreement was expected, because independent refinements indicated that the common variables (Δr for the U–Na, U–Ca, and U–O_{dist} signals) overlap within the uncertainties in the EXAFS measurement. The best-fit values for the distances from U to Na, Ca, and O_{dist} are 3.85 ± 0.02 Å, 4.01 ± 0.01 Å, and 4.10 ± 0.04 Å, respectively. The spectrum without Ca, Ca0a, was modeled with an independent U to Na distance that was optimized to the value of 3.82 ± 0.01 Å. The best-fit values for N_{Ca} and N_{Na} are listed in Table 5. Fitting the data series with a single model enables determination of the number of calcium atoms to approximately ± 0.6 atom (see Table 5) for the highest [Ca] (Ca5000a, and Ca5000). Although the EXAFS uncertainties are still large, the values and trends for N_{Ca} and N_{Na} are similar for the EXAFS and equilibrium aqueous speciation calculation approaches (Fig. 6). The speciation calculations based on Bernhard et al. (2001) (Model A) and Dong and Brooks, 2006 (Model B) are similar (see Table 2 and Fig. 6). The EXAFS results are somewhat in better agreement with Model B for the number of Na atoms at the highest Ca concentrations.

To further illustrate that the numbers of sodium and calcium atoms determined from this fitting model depend weakly on the equatorial oxygen coordination number, we performed an EXAFS modeling comparison by holding the number of equatorial oxygen atoms in the model described above at a value of 6 (as previously justified on the basis of the aqueous speciation calculations shown in Table 2). Additional EXAFS modeling tests were

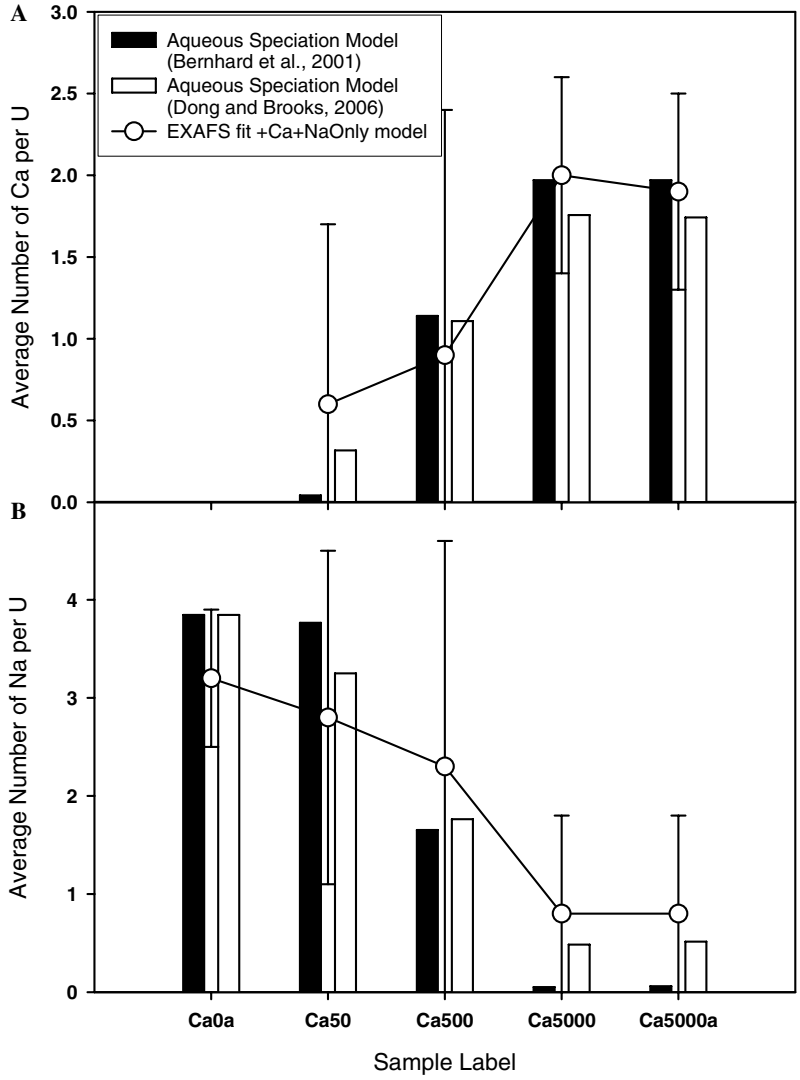

Fig. 6. Predicted average values for N_{Ca} (A) and N_{Na} (B) from equilibrium aqueous speciation modeling and as determined by modeling of EXAFS data.

performed by holding the number of equatorial oxygen atoms at a value of 5 (one atom less than in the current model) or at a value of 7 (one atom more than in the current model). The fit results with the number of equatorial oxygen atoms held at values of 5 and 7 were fully consistent with the values reported for the current model with the number of equatorial oxygen atoms held at a value of 6 (Table 5, Model +Ca+NaOnly). For example, the best-fit value for the number of sodium atoms from the Ca0a data set were determined to be 3.2 ± 0.7, 3.2 ± 0.7, and 3.3 ± 0.7 for the models with the number of equatorial oxygen atoms held at values of 5, 6, and 7, respectively. In addition, the best-fit values for the number of calcium atoms for the Ca5000 data set were determined to be 2.5 ± 0.5, 2.0 ± 0.6, and 1.6 ± 0.6 for the models with the number of equatorial oxygen atoms held at values of 5, 6, and 7, respectively. These tests explicitly show that the numbers of calcium and sodium atoms depend weakly on the equatorial oxygen coordination number, increasing confidence in the results obtained from the model that holds the equatorial oxygen coordination number at 6.

Qualitatively, the amplitudes of the magnitude and real parts of the FT in Fig. 5 within the region from 2.9 to 4.0 Å show increasing calcium signal as the calcium concentration increased from 0 to 5000 μM. This signal became apparent when the FT of the same data set was compared with different k weights. To make this comparison, the first-shell oxygen signals were normalized to the same amplitude. If all the signals in the EXAFS data are from atoms with atomic number similar to the first oxygen shell, then the relative amplitudes of all the signals will follow that of the first shell. Hence, the FT spectra for data with k weights 1, and 2, and 3 will overplot. This is illustrated for the Ca0a and Ca50 data sets by the plots in Fig. 5, as the signal in the region from 2.9 to 4.0 Å is similar for all three k weights. As the atomic number of a neighboring atom becomes greater than that of oxygen, the calcium signal will increase in amplitude as the k weight increases from 1 to 3. This trend is clearly indicated for the Ca500 and Ca5000 data sets shown in Fig. 5. These data sets have a Fourier-transformed data range of 3.5–9.5 $Å^{-1}$. The data within the range of higher k values, from approximately 7 to 9.5 $Å^{-1}$, are dominated by the calcium signal, so that the FT with a k weight of 3 (rather than a k weight of 1) will emphasize the calcium signal. The Ca5000a data set does not show this trend because of the limited data range of the FT, from 3.5 to 7.5 $Å^{-1}$. This qualitative comparison of the Fourier-transformed data further supports the inclusion of sodium complexation at the lower calcium concentrations to explain the amplitudes of the magnitude and real parts of the FT within the region from ~2.9 to 4.0 Å and coordination number trends as a function of calcium concentration.

4. Conclusions

A relatively simple molecular species Na/Ca–UO_2–CO_3 can demand a relatively complicated EXAFS model (Table 3). In the present analysis of a series of EXAFS data and qualitative comparison of the k dependence of the FT of the EXAFS data, inclusion of the Na–UO_2–CO_3 complex in the model was necessary to achieve a dependence on calcium concentration for the N_{Ca} and N_{Na}, as expected based on equilibrium aqueous speciation calculations (Table 2). Values for N_{Ca} were determined to be 0.6 ± 1.1, 0.9 ± 1.5, 2.0 ± 0.6, and 1.9 ± 0.6 for the solutions containing calcium concentrations of 50, 500, 5000, and 5000 μM, respectively. Values for N_{Na} were determined to be 3.2 ± 0.7, 2.8 ± 1.7, 2.3 ± 2.3, and 0.8 ± 1.0 for solutions Ca0a, Ca50, Ca500, and Ca5000/Ca5000a. Even though a mixture of Ca–UO_2–CO_3 and Ca_2–UO_2–CO_3 species seems likely (e.g., (Dong and Brooks, 2006)) and the present analysis reduced the uncertainty in N_{Ca} to approximately ±0.6 calcium atom for the spectra from the highest [Ca], determination of the exact stoichiometry of the complex remains difficult. On the average, approximately 2 calcium atoms are bound to the uranyl carbonate species at the highest concentrations and 2–4 sodium atoms are bound to the uranyl carbonate species when calcium is absent.

The final EXAFS results for the average values of N_{Ca} and N_{Na} in these solutions are reasonable and in agreement with speciation calculations (Fig. 6). The EXAFS results for the number of sodium atoms at the highest calcium concentrations agree better with the Model B results than with the Model A results. Model B incorporates the formation constants proposed by Dong and Brooks (2006) which suggest a more prominent role for the $CaUO_2(CO_3)_3^{2-}$ complex. Consequently, model results obtained with these constants will also predict a higher average number of sodium per U with the assumption that the charge of the $CaUO_2(CO_3)_3^{2-}$ species is satisfied by two sodium ions. Under these same conditions, Model A does not predict a significant $CaUO_2(CO_3)_3^{2-}$ species, and hence the cation charge of the extended uranyl moiety is fully satisfied by calcium alone. The EXAFS model unconstrained by charge balance considerations, minimizes the residual error between model and data and allows for independent measurement of the average number of calcium and sodium atoms per uranyl atom. The dominance of the $CaUO_2(CO_3)_3^{2-}$ species at environmentally relevant conditions is a discovery of the Dong and Brooks (2006) study that is supported by our EXAFS measurements.

Because of the overlap of signals from the O_{dist}, calcium, and sodium atoms, σ^2 values for a liebigite crystal structure were used to model the solution series. If the σ^2 values (mean-squared deviation of the distance between the uranium atom and the calcium atoms) are similar for the aqueous solution and the crystal structure, one must ask whether the stabilities of the atoms about their local minima in a crystal structure are affected by long-range order. Our EXAFS results indicate that σ^2 values determined through modeling of EXAFS data from a crystal can be used to model EXAFS data from a solution; thus, the stability of the aqueous species may be similar to that of the

fully incorporated species bound within a crystal structure. Hence, the bond strength might be similar in the aqueous complex and in an extended crystal structure. The similarity in the bond strength of the aqueous and solid phases would help to explain the strength of the formation constant $\log K \sim 30$ (Bernhard et al., 1996) for this complex, the pronounced effect of the complex on the bioreducibility of uranium(VI) (Brooks et al., 2003), and the increased transport properties attributed to the formation of the complex (Brooks et al., 2003; Zheng et al., 2003).

This study of calcium-uranyl-carbonate species at environmentally relevant concentrations with groundwater components of calcium and sodium, conducted with a combination of X-ray absorption spectroscopy and aqueous equilibrium speciation calculations, has potential for determining the predominant aqueous species and the stability of these species through modeling of XAFS-measured σ^2 values. An understanding of uranyl aqueous species in environmentally relevant groundwater—where the transport properties are dictated by molecular interactions of aqueous species with groundwater components—is critical to accurate predictions of contaminant transport within the subsurface, before and as a result of remediation strategies.

Acknowledgments

This work was supported by the U.S. Department of Energy (DOE), Office of Science, Office of Biological and Environmental Research, Environmental Remediation Sciences Program. MRCAT operations are supported by the U.S. DOE and the MRCAT member institutions. Advance Photon Source is supported by the U.S. DOE, Office of Science, Office of Basic Energy Sciences, under contract W-31-109-ENG-38. Special appreciation is extended to E.J. O'Loughlin and M. Boyanov for assistance with the uranium XAFS data collection. Finally, the authors wish to thank William M. Murphy and two anonymous reviewers for their insightful review comments.

Associate editor: David J. Wesolowski

References

Allen, P.G., Bucher, J.J., Clark, D.L., Edelstein, N.M., Ekberg, S.A., Gohdes, J.W., Hudson, E.A., Kaltsoyannis, N., Lukens, W.W., Neu, M.P., Palmer, P.D., Reich, T., Shuh, D.K., Tait, C.D., Zwick, B.D., 1995. Multinuclear NMR, Raman, EXAFS, and X-ray-diffraction studies of uranyl carbonate complexes in near-neutral aqueous-solution: X-ray structure of $[C(NH_2)3]_6[(UO_2)_3(CO_3)_6]6.5H_2O$. *Inorg. Chem.* **34**, 4797–4807.

Anderson, R.T., Vrionis, H.A., Ortiz-Bernad, I., Resch, C.T., Long, P.E., Dayvault, R., Karp, K., Marutzky, S., Metzler, D.R., Peacock, A., White, D.C., Lowe, M., Lovley, D.R., 2003. Stimulating the in situ activity of *Geobacter* species to remove uranium from the groundwater of a uranium-contaminated aquifer. *Appl. Environ. Microbiol.* **69**, 5884–5891.

Bailey, E.H., Mosselmans, J.F.W., Schofield, P.F., 2005. Uranyl-citrate speciation in acidic aqueous solutions—an XAS study between 25 and 200 °C. *Chem. Geol.* **216**, 1–16.

Bargar, J.R., Reitmeyer, R., Lenhart, J.J., Davis, J.A., 2000. Characterization of U(VI)-carbonato ternary complexes on hematite: EXAFS and electrophoretic mobility measurements. *Geochim. Cosmochim. Acta* **64**, 2737–2749.

Bernhard, G., Geipel, G., Brendler, V., Nitsche, H., 1996. Speciation of uranium in seepage waters of a mine tailing pile studied by time-resolved laser-induced fluorescence spectroscopy (TRLFS). *Radiochim. Acta* **74**, 87–91.

Bernhard, G., Geipel, G., Reich, T., Brendler, V., Amayri, S., Nitsche, H., 2001. Uranyl(VI) carbonate complex formation: Validation of the $Ca_2UO_2(CO_3)_{3aq.}$ species. *Radiochim. Acta* **89**, 511–518.

Bethke, C.M., 2005. *The Geochemist's Workbench Release 6.0 GWB Reaction Modeling Guide*. Rockwater, Inc., Golden, CO.

Bevington, P.R., Robinson, D.K., 1992. *Data Reduction and Error Analysis for the Physical Sciences*. McGraw-Hill, New York.

Bostick, B.C., Fendorf, S., Barnett, M.O., Jardine, P.M., Brooks, S.C., 2002. Uranyl surface complexes formed on subsurface media from DOE facilities. *Soil Sci. Soc. Am. J.* **66**, 99–108.

Brooks, S.C., Fredrickson, J.K., Carroll, S.L., Kennedy, D.W., Zachara, J.M., Plymale, A.E., Kelly, S.D., Kemner, K.M., Fendorf, S., 2003. Inhibition of bacterial U(VI) reduction by calcium. *Environ. Sci. Technol.* **37**, 1850–1858.

Catalano, J.G., Brown, G.E., 2004. Analysis of uranyl-bearing phases by EXAFS spectroscopy: interferences, multiple scattering, accuracy of structural parameters, and spectral differences. *Am. Mineral.* **89**, 1004–1021.

Coda, A., Della Giusta, A., Tazzoli, V., 1981. The structure of synthetic Andersonite $Na_2Ca[UO_2(CO_3)3]{\cdot}xH_2O$ $x \sim 5.6$. *Acta Cryst.* **B37**, 1496–1500.

Davis, J.A., Meece, D.E., Kohler, M., Curtis, G.P., 2004. Approaches to surface complexation modeling of uranium(VI) adsorption on aquifer sediments. *Geochim. Cosmochim. Acta* **68**, 3621–3641.

Dodge, C.J., Francis, A.J., 2003. Structural characterization of a ternary Fe(III)–U(VI)–citrate complex. *Radiochim. Acta* **91**, 525–532.

Dong, W.M., Brooks, S.C., 2006. Determination of the formation constants of ternary complexes of uranyl and carbonate with alkaline earth metals (Mg^{2+}, Ca^{2+}, Sr^{2+}, and Ba^{2+}) using anion exchange method. *Environ. Sci. Technol.* **40**, 4689–4695.

Duff, M.C., Amrhein, C., 1996. Uranium(VI) adsorption on goethite and soil in carbonate solutions. *Soil. Sci. Soc. Am. J.* **60**, 1393–1400.

Duff, M.C., Amrhein, C., Bradford, G., 1997. Nature of uranium contamination in the agricultural drainage water evaporation ponds of the San Joaquin Valley, California, USA. *Can. J. Soil Sci.* **77**, 459–467.

Duff, M.C., Coughlin, J.U., Hunter, D.B., 2002. Uranium co-precipitation with iron oxide minerals. *Geochim. Cosmochim. Acta* **66**, 3533–3547.

Elzinga, E.J., Tait, C.D., Reeder, R.J., Rector, K.D., Donohoe, R.J., Morris, D.E., 2004. Spectroscopic investigation of U(VI) sorption at the calcite–water interface. *Geochim. Cosmochim. Acta* **68**, 2437–2448.

Fredrickson, J.K., Zachara, J.M., Kennedy, D.W., Liu, C.X., Duff, M.C., Hunter, D.B., Dohnalkova, A., 2002. Influence of Mn oxides on the reduction of uranium(VI) by the metal-reducing bacterium *Shewanella putrefaciens*. *Geochim. Cosmochim. Acta* **66**, 3247–3262.

Fuller, C.C., Bargar, J.R., Davis, J.A., Piana, M.J., 2002. Mechanisms of uranium interactions with hydroxyapatite: implications for groundwater remediation. *Environ. Sci. Technol.* **36**, 158–165.

Gorby, Y.A., Lovley, D.R., 1992. Enzymatic uranium precipitation. *Environ. Sci. Technol.* **26**, 205–207.

Grenthe, I., Fuger, J., Konings, R.J.M., Lemire, R.J., Muller, A.B., Cregu, C.N.T., Wanner, H., 1992. *Chemical Thermodynamics of Uranium*. North-Holland Elsevier Science, New York.

Guillaumont, R., Franghanel, T., Fuger, J., Grenthe, I., Neck, V., Palmer, D.A., Rand, M.H., 2003. *Update on The Chemical Thermodynamics of Uranium, Neptunium, Plutonium, Americium and Technetium*. Elsevier, Amsterdam.

Istok, J.D., Senko, J.M., Krumholz, L.R., Watson, D., Bogle, M.A., Peacock, A., Chang, Y.J., White, D.C., 2004. In situ bioreduction of technetium and uranium in a nitrate-contaminated aquifer. *Environ. Sci. Technol.* **38**, 468–475.

Kalmykov, S.N., Choppin, G.R., 2000. Mixed $Ca^{2+}/UO_2^{2+}/CO_3^{2-}$ complex formation at different ionic strengths. *Radiochim. Acta* **88**, 603–606.

Kelly, S.D., Newville, M.G., Cheng, L., Kemner, K.M., Sutton, S.R., Fenter, P., Sturchio, N.C., Spotl, C., 2003. Uranyl incorporation in natural calcite. *Environ. Sci. Technol.* **37**, 1284–1287.

Kelly, S.D., Rasbury, E.T., Chattopardhyay, S., Kropf, A.J., Kemnner, K.M., 2006. Evidence of a stable uranyl site in ancient organic-rich calcite. *Environ. Sci. Technol.* **40**, 2262–2268.

Langmuir, D., 1978. Uranium solution-mineral equilibria at low temperatures with applications to sedimentary ore deposits. *Geochim. Cosmochim. Acta* **42**, 547–569.

Lovley, D.R., 2003. Cleaning up with genomics: applying molecular biology to bioremediation. *Nat. Rev. Microbiol.* **1**, 35–44.

Lovley, D.R., Phillips, E.J.P., 1992. Reduction of uranium by *Desulfovibrio–Desulfuricans. Appl. Environ. Microb.* **58**, 850–856.

Lovley, D.R., Phillips, E.J.P., Gorby, Y.A., Landa, E.R., 1991. Microbial reduction of uranium. *Nature* **350**, 413–416.

Mereiter, K., 1982. The crystal structure of Liebigite, $Ca_2UO_2(CO_3)_3{\cdot}11\text{-}H_2O$. *Tschermaks Min. Petr. Mitt.* **30**, 277–288.

Morse, J.W., Shanbhag, P.M., Saito, A., Choppin, G.R., 1984. Interaction of uranyl ions in carbonate media. *Chem. Geol.* **42**, 85–99.

Newville, M., 2001. IFEFFIT: interactive EXAFS analysis and FEFF fitting. *J. Synch. Rad.* **8**, 322–324.

Newville, M., Livinš, P., Yacoby, Y., Rehr, J.J., Stern, E.A., 1993. Near-edge X-ray absorption fine structure of Pb: a comparison of theory and experiment. *Phys. Rev. B* **47**, 14126–14131.

Newville, M., Boyanov, B.I., Sayers, D.E., 1999. Estimation of uncertainties in XAFS data. *J. Synch. Rad.* **6**, 264–265.

Ondrus, P., Skala, R., Veselovsky, F., Sejkora, J., Vitti, C., 2003. Cejkaite, the triclinic polymorph of $Na_4(UO_2)(CO_3)_3$—a new mineral from Jachymov, Czech Republic. *Am. Mineral* **88**, 686–693.

Rakovan, J., Reeder, R.J., Elzinga, E.J., Cherniak, D.J., Tait, C.D., Morris, D.E., 2002. Structural characterization of U(VI) in apatite by X-ray absorption spectroscopy. *Environ. Sci. Technol.* **36**, 3114–3117.

Ravel, B., Newville, M., 2005. Athena, Artemis, Hephaestus: data analysis for X-ray absorption spectroscopy using IFEFFIT. *J. Synch. Rad.* **12**, 537–541.

Reeder, R.J., Nugent, M., Lamble, G.M., Tait, C.D., Morris, D.E., 2000. Uranyl incorporation into calcite and aragonite: XAFS and luminescence studies. *Environ. Sci. Technol.* **34**, 638–644.

Reeder, R.J., Nugent, M., Tait, C.D., Morris, D.E., Heald, S.M., Beck, K.M., Hess, W.P., Lanzirotti, A., 2001. Coprecipitation of uranium(VI) with calcite: XAFS, micro-XAS, and luminescence characterization. *Geochim. Cosmochim. Acta* **65**, 3491–3503.

Reich, T., Moll, H., Arnold, T., Denecke, M.A., Hennig, C., Geipel, G., Bernhard, G., Nitsche, H., Allen, P.G., Bucher, J.J., Edelstein, N.M., Shuh, D.K., 1998. An EXAFS study of uranium(VI) sorption onto silica gel and ferrihydrite. *J. Electron Spectrosc.* **96**, 237–243.

Segre, C.U., Leyarovska, N.E., Chapman, L.D., Lavender, W.M., Plag, P.W., King, A.S., Kropf, A.J., Bunker, B.A., Kemner, K.M., Dutta, P., Druan, R.S., Kaduk, J., 2000. The MRCAT insertion device beamline at the advanced photon source. *Synchrotron Rad. Inst. CP521*, 419–422.

Shock, E.L., Koretsky, C.M., 1993. Metal-organic complexes in geochemical processes—calculation of standard partial molal thermodynamic properties of aqueous acetate complexes at high-pressures and temperatures. *Geochim. Cosmochim. Acta* **57**, 4899–4922.

Stern, E.A., 1974. Theory of the extended X-ray-absorption fine structure. *Phys. Rev. B* **10**, 3027–3037.

Stern, E.A., Heald, S.M., 1983. Basic principles and applications of EXAFS. In: Koch, E.E. (Ed.), *Handbook of Synchrotron Radiation*. North-Holland, New York.

Stern, E.A., Newville, M., Ravel, B., Yacoby, Y., Haskel, D., 1995. The UWXAFS analysis package: philosophy and details. *Phys. B* **208 & 209**, 117–120.

Sturchio, N.C., Antonio, M.R., Soderholm, L., Sutton, S.R., Brannon, J.C., 1998. Tetravalent uranium in calcite. *Science* **281**, 971–973.

Suzuki, Y., Kelly, S.D., Kemner, K.M., Banfield, J.F., 2004. Enzymatic U(VI) reduction by *Desulfosporosinus* species. *Radiochim. Acta* **92**, 11–16.

Tokunaga, T.K., Wan, J.M., Pena, J., Sutton, S.R., Newville, M.G., 2004. Hexavalent uranium diffusion into soils from concentrated acidic and alkaline solutions. *Environ. Sci. Technol.* **38**, 3056–3062.

U.S. Department of Energy (2000) Environmental assessment for selection and operation of the proposed field research centers, public.ornl.gov/nabirfrc.

Waite, T.D., Davis, J.A., Payne, T.E., Waychunas, G.A., Xu, N., 1994. Uranium(VI) adsorption to ferrihydrite—application of a surface complexation model. *Geochim. Cosmochim. Acta* **58**, 5465–5478.

Zabinsky, S.I., Rehr, J.J., Ankudinov, A., Albers, R.C., Eller, M.J., 1995. Multiple-scattering calculations of X-ray-absorption spectra. *Phys. Rev. B* **52**, 2995–3009.

Zheng, Z.P., Tokunaga, T.K., Wan, J.M., 2003. Influence of calcium carbonate on U(VI) sorption to soils. *Environ. Sci. Technol.* **37**, 5603–5608.